Solar Energy Materials & Solar Cells 166 (2017) 121–126

Contents lists available at ScienceDirect

Solar Energy Materials & Solar Cells

journal homepage: www.elsevier.com/locate/solmat

18.87%-efficient inverted pyramid structured silicon solar cell by one-step Cu-assisted texturization technique

Lixia Yang[a], Yaoping Liu[a,*], Yan Wang[a], Wei Chen[a], Quansheng Chen[a], Juntao Wu[a], Andrej Kuznetsov[b], Xiaolong Du[a,*]

[a] Key Laboratory for Renewable Energy, Beijing Key Laboratory for New Energy Materials and Devices, National Laboratory for Condensed Matter Physics, Institute of Physics, Chinese Academy of Sciences, Beijing 100190, China
[b] Department of Physics, Centre for Materials Science and Nanotechnology, University of Oslo, PO Box 1048 Blindern, Oslo NO-0316, Norway

ARTICLE INFO

Keywords:
Cu-assisted texturization
Inverted pyramid
Light-trapping
Silicon solar cells

ABSTRACT

We achieved an inverted pyramid structure, meeting the tradeoff between the light reflection minimization and carrier recombination by adjusting the one-step Cu-assisted texturization of silicon wafer, and silicon solar cells based on this structure were fabricated, which gained a high conversion efficiency of 18.87% without using any complex techniques. These data were compared with the performance of conventional upright pyramid silicon solar cells as manufactured using identical raw wafers, the Cu-etched inverted pyramid silicon cells collected 0.59 mA/cm^2 more short-circuit current density and 0.47% more efficiency. Importantly, our data demonstrate the better performance and manufacturability of inverted pyramid structured silicon solar cell and as such may open new perspectives for high efficiency solar cell applications.

1. Introduction

Metal-assisted chemical etching has been widely used for fabricating black silicon (B-Si), and there has been significant interest in using this B-Si as an antireflection (AR) coating for Si solar cells not only because of its superior AR effect but also the cost savings and simplicity during mass production [1–7]. B-Si solar cells with efficiency of 17.1% and 18.2% were achieved by Au and Ag-assisted chemical etching, respectively [5,8]. In contrast to Au and Ag, the Cu-assisted chemical etching is more promising for commercial fabrication of Si solar cells because of its much lower cost [9,10]. Nevertheless, although such Cu-assisted chemical etching method has the cost advantage, this method has yet to be commercialized because Cu^{2+}/Cu exhibit much lower redox potential, poorly matching the valence band of Si [3]. In the previous Cu-etched works, only shallow pits were demonstrated [11–13], or with increased etching time Cu tends to form a dense film on the Si surface [14], which will hinder the etching of Si, making it impossible to obtain B-Si. Recently, by introducing H_3PO_3 to the etching solution as a reducing agent and extending the etching time to 8 h, Lu *et al.* synthesized inverted pyramid nanopore-type B-Si with low mean reflectivity of 0.96% at room temperature [15]. Toor *et al.* finally achieved B-Si with mean reflectivity of 3.1% by rising the etching temperature to 50 °C via two-steps Cu-assisted chemical etching method. They also fabricated a solar cell with a conversion efficiency of 17.0% using Cu-etched nanoporous B-Si on pyramidal-textured Si substrate [16]. It should be noted that the B-Si for commercial solar cells fabricated by the above Au, Ag or Cu-assisted etching methods can only be obtained on polished, pyramidal-structured or other textured Si substrate, but not raw Si, because the saw damage layer can't be totally removed during the etching process.

As a result of our recent work, inverted pyramid structures, instead of above-mentioned nanostructures, were fabricated by one-step maskless Cu-assisted texturization of the raw Si [17]. This Cu-etched method can efficiently remove the saw damage layer on raw Si and form inverted pyramids. Moreover, this inverted pyramid structured Si will avoid severe recombination losses encountered by the nanostructured B-Si thanks to its big and open structure characteristic. The surface area of the micrometer-scale inverted pyramids is almost the same as that of pyramids, indicating that the surface passivation for our inverted pyramids is not more difficult than that for pyramids, but much easier than that for nanostructured one. Importantly, in addition to the low reflectivity superiority, these inverted pyramid structures are characterized with recessed and wide deeps, making this texture very applicable for conformal coating and filling, such as for the coverage of SiN_x and the filling of metal electrodes in photovoltaic devices [18]. Except for these superior structure characteristics, our inverted pyramid fabrication is proceeded at 50 °C for about 15 min, reducing the energy consumption and time cost in comparison with the upright

* Corresponding authors.
E-mail addresses: ypliu@iphy.ac.cn (Y. Liu), xldu@iphy.ac.cn (X. Du).

http://dx.doi.org/10.1016/j.solmat.2017.03.017
Received 6 June 2016; Received in revised form 22 November 2016; Accepted 16 March 2017

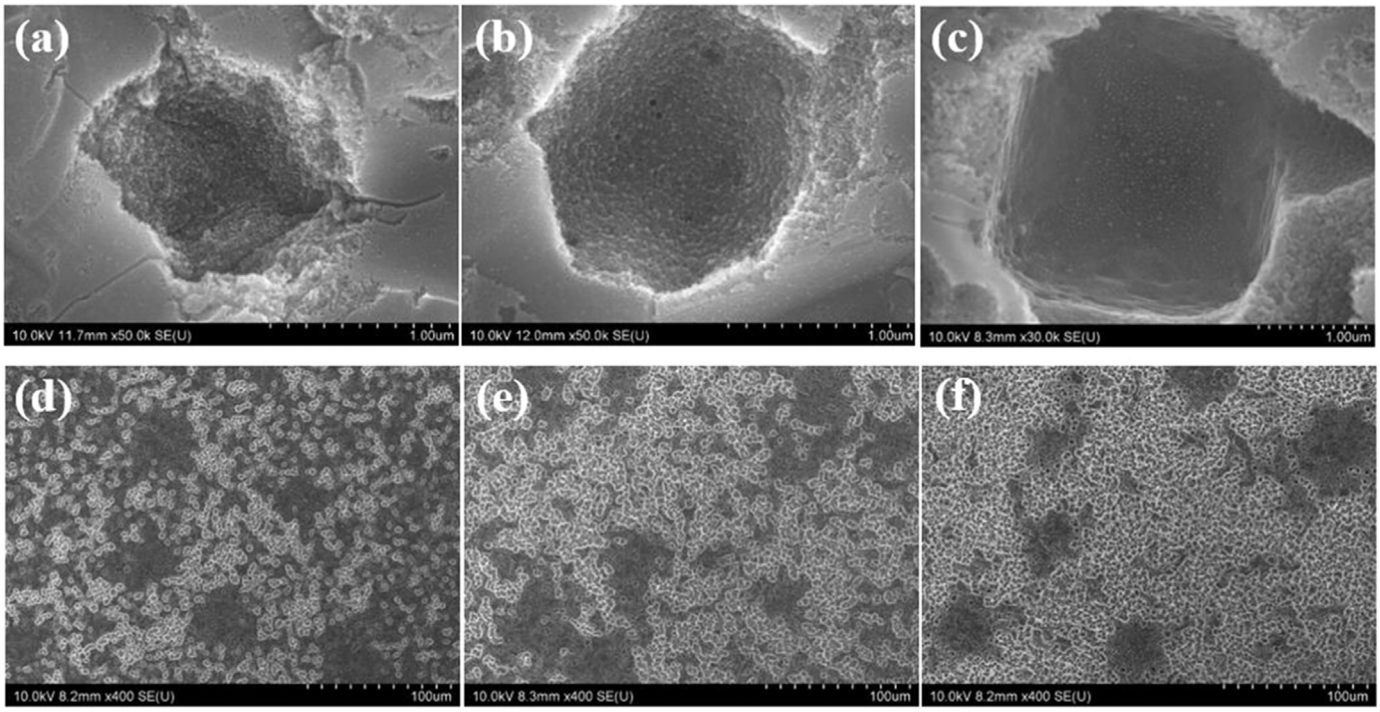

Fig. 1. SEM images of the inverted pyramid structures for **(a)** and **(d)** 5 s processing, **(b)** and **(e)** 25 s processing, **(c)** and **(f)** 60 s processing.

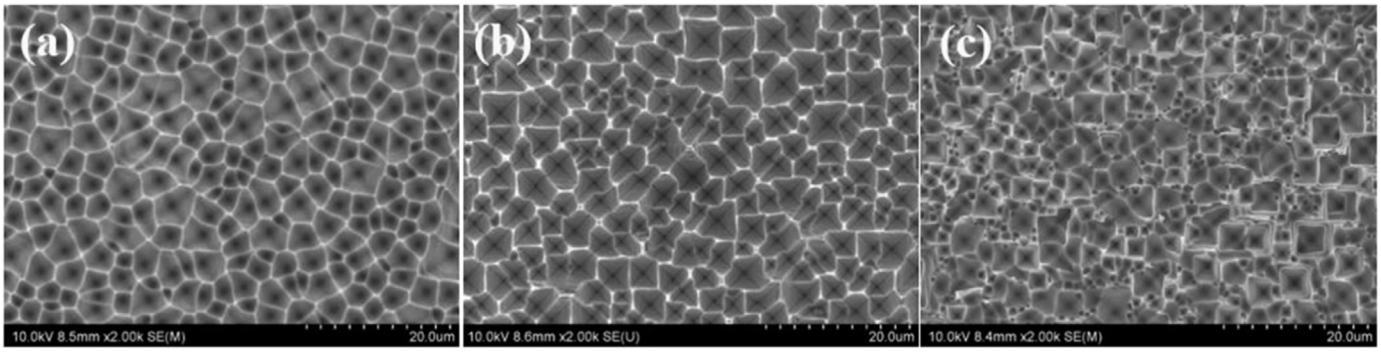

Fig. 2. SEM images of the inverted pyramid structures for **(a)** 10 min processing, **(b)** 15 min processing and **(c)** 20 min processing.

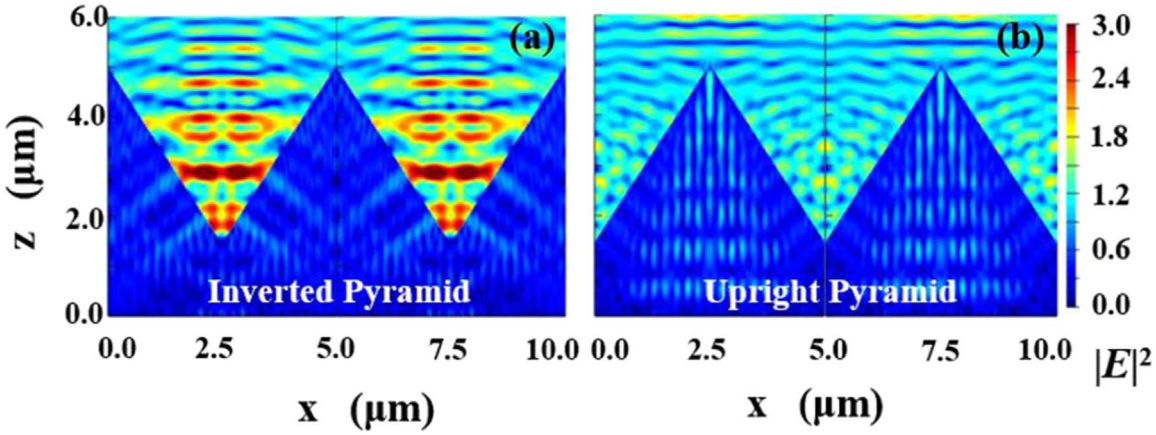

Fig. 3. FDTD simulation results of the electric field intensity distributions in **(a)** inverted pyramid structured Si and **(b)** upright pyramid structured Si.

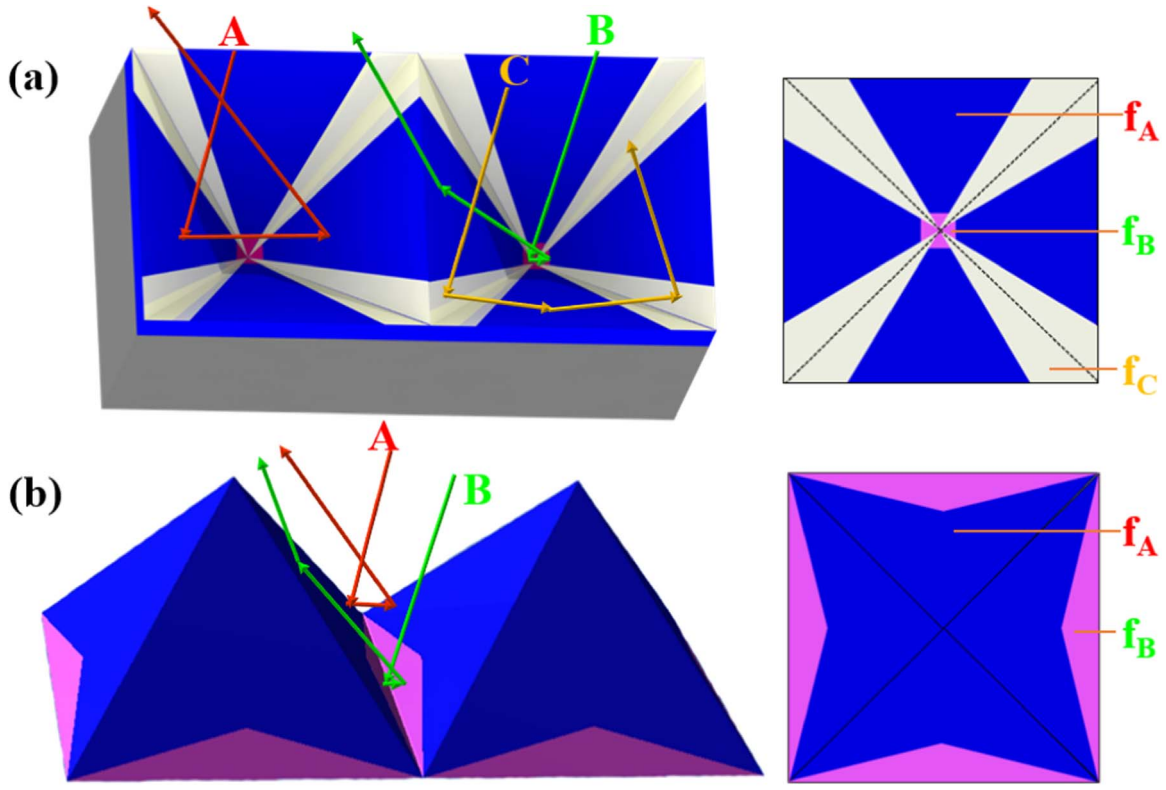

Fig. 4. Possible reflection paths of the normally incident rays from **(a)** inverted pyramid structured Si and **(b)** upright pyramid structured Si. Shown on the images are the pyramid facets struck by rays reflected along paths A, B and C. The various area proportions were used to determine f_A (the blue color area), f_B (the pink color area), and f_C (the light yellow color area). (For interpretation of the references to color in this figure legend, the reader is referred to the web version of this article.).

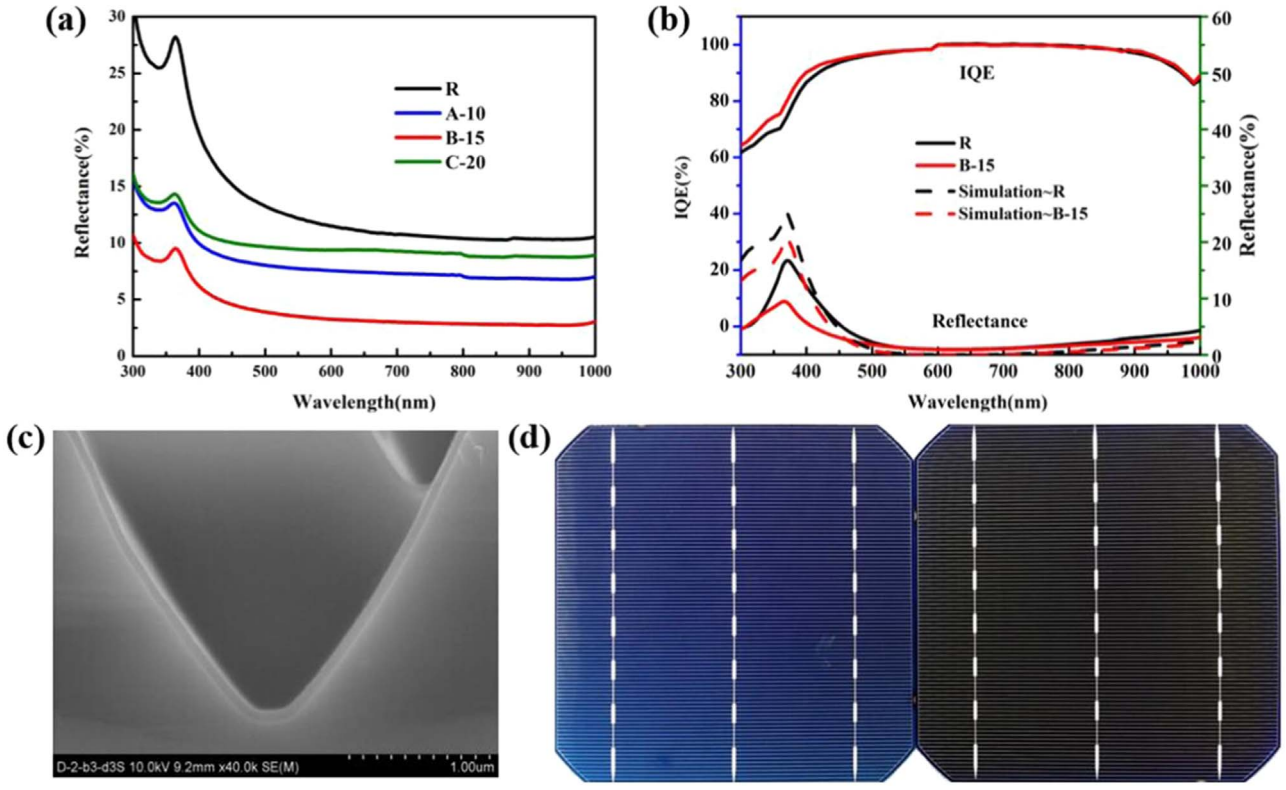

Fig. 5. (a) Reflectance spectra of sample R, A-10, B-15 and C-20, **(b)** IQE and reflectance spectra of sample R and B-15 with 80 nm SiN_x by 3D ray tracing simulations and experiments, **(c)** cross-sectional SEM image of the interface between SiN_x and the inverted pyramid structured Si and **(d)** images of solar cells based on upright pyramids(left) and inverted pyramids(right). (For interpretation of the references to color in this figure, the reader is referred to the web version of this article.).

Table 1
Summary of performance for the inverted pyramid structured and upright pyramid structured Si solar cells. Performance metrics reported are the average of 5 cells.

Sample	V_{oc} (mV)	J_{sc} (mA/cm^2)	FF (%)	E_{ff} (%)	R_s (ohm)	
A–10	637.1	36.94	79.01	18.62	0.00219	Best
	636.3	36.95	78.67	18.52	0.00224	Average
B–15	637.7	37.47	78.84	18.87	0.00250	Best
	636.6	37.49	78.81	18.83	0.00242	Average
C–20	633.8	36.92	78.24	18.34	0.00241	Best
	634.2	36.62	78.62	18.28	0.00245	Average
R	637.0	36.88	78.22	18.40	0.00275	Best
	634.7	36.84	77.87	18.23	0.00277	Average

pyramid fabrication, and making it very facile to combine with the current industry.

In this work, we utilize Cu nanoparticles (NPs) to catalyze chemical etching of Si for high performance solar cells. The formation process of the inverted pyramid structures and the performance of the solar cells based on this structure are investigated systematically. We also fabricate a series of Si solar cells based on inverted pyramid structures which were fabricated by Cu-assisted texturization technique for 10 min, 15 min and 20 min. A conversion efficiency as high as 18.87% is achieved with large area of 156 mm×156 mm, which shows the best performance in the conventional Si solar cells based on Cu-etched method. Our technique, compatible with current production line, is low-cost and simple, which may trigger a new era of solar cells based on inverted pyramid structured Si.

2. Experimental

Commercial 200 μm thick 156 mm×156 mm (100)-oriented crystalline silicon (c-Si), boron-doped (1–3 Ω cm) p-type wafers were used in the study. Inverted pyramid structured Si was fabricated using a maskless Cu-NPs assisted anisotropic chemical etching technique. Before etching, the Si wafers were cleaned by acetone, ethanol, and deionized water and dried by N_2 gas. Then the Si wafers were immersed in a polytetrafluoroethene container which was filled with 0.005 M $Cu(NO_3)_2$, 4.6 M HF and 0.55 M H_2O_2 for 10 min, 15 min and 20 min at 50 ℃ [17], labeled as sample A-10, B-15 and C-20, respectively. Residual Cu-NPs were removed by concentrated HNO_3 in a sonication bath for 20 min and the nanostructures at the surface were removed by dipping the samples into the 2 wt% KOH and 5 wt% IPA solution mixing for 1 min. Finally the samples were rinsed with deionized water and dried by blowing N_2. Furthermore, upright pyramid structured Si was prepared with a standard anisotropic alkaline etching recipe described elsewhere [19] for reference, labeled as sample R. Conventional diffused-junction Si solar cell process was used to fabricate inverted pyramid structured Si and upright pyramid structured Si solar cells. After standard RCA cleaning, the n^+-emitter was formed by phosphorus diffusion using a $POCl_3$ source, which obtained a sheet resistance of ~80 Ω/sq. The phosphosilicate glass that formed during $POCl_3$ diffusion was removed with 5 vol% HF for 120 s. An 80 nm SiN_x layer was then formed by PECVD to passivate the surface. Back metal contacts were made by applying aluminium paste and alloying at 840 ℃ for 4 s. For the front metal contact, the desired Ag-based grid pattern was screen printed and firing at 840 ℃ for 4 s.

The morphologies and structures of the samples were characterized with a Hitachi S-4800 scanning electron microscope. Hemispheric total reflectance for normal incidence was measured on a Varian Cary 5000 spectrophotometer with an integrating sphere. The lifetime of the minority carriers was measured by using a Sinton WCT-120. The cell efficiency was measured by using a BERGER Lichttechnik Single Cell Tester and the quantum efficiency was measured by using a Solar Cell Spectral Response/QE/IPCE Measurement System QEX10.

3. Results and discussion

We perform a systematic study of the inverted pyramid structure obtained by simple and low-cost Cu-NPs assisted chemical etching of Si at 50 ℃. The underlying principles are based on the electrochemical reaction between Si and Cu^{2+}/Cu, which have been systematically studied in our previous work [17]. Fig. 1(a), (b) and (c) show the early forms of an inverted pyramid via etching for 5 s, 25 s and 60 s at high magnification, while the morphology transitions of large-area range during the reaction are shown in Fig. 1(d), (e) and (f) at low magnification. As shown in Fig. 1(a), we notice that Cu^{2+} ions preferentially capture electrons from the kinks and steps of Si substrate and Cu-NPs originally adsorb there due to the surface free energy is much higher there than the flat areas [20]. The pit is becoming larger and deeper by Cu-assisted etching for 25 s, as shown in Fig. 1(b). When etching time prolongs to 60 s, see Fig. 1(c), where more and larger Cu-NPs are observed on Si (100) surface and fewer and smaller Cu-NPs are observed on Si (111) surfaces, the original induced pit is becoming square shaped due to the anisotropic deposition of Cu-NPs, further catalyzing anisotropic etching, which is obviously different from the deposition of Au-NPs and Ag-NPs [15,17]. In fact, due to a much weaker electron capturing ability of Cu^{2+} than that of Ag^+, and a difference of electron supplying rates in Si (100) and (111) planes, Cu-NPs population on c-Si appear to be anisotropic, which will induce an anisotropic etching and the formation of inverted pyramid [17]. The inverted pyramid is becoming standard and bestrewing fast over time,

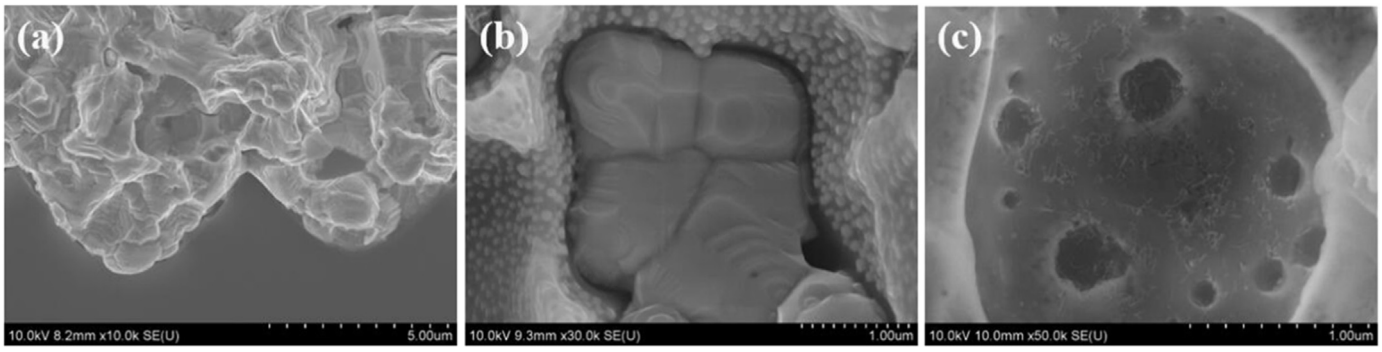

Fig. 6. SEM images of Ag electrode contact with inverted pyramid structured Si **(a)** cross-sectional view, **(b)** top-view and **(c)** SEM image of Ag crystallites in the emitter region after immersing in nitric acid solution for 5 min.

as shown in Fig. 1(d), (e), (f).

When the etching time is increased to 10 min, 15 min and 20 min, as shown in Fig. 2, we see a clear stage from formation to collapse of the inverted pyramid structures. Fig. 2(a) is an SEM image of sample A-10, showing an array of shallow inverted-pyramid-like structures, the joint between Si (111) planes is still rounded, indicating an original formation stage. With longer etching time, the inverted pyramids of sample B-15 are becoming more standard with Si (111) sidewalls, as shown in Fig. 2(b). The length of the inverted pyramids' bottom side varies within 3–7 μm, and the etching depth is in the range of 2–5 μm. Moreover, the Si surface is fully covered by the random inverted pyramids, indicating an optimization stage. When the etching time was too long, 20 min for example, the standard inverted pyramid structure was overetched and became shallow, as shown in Fig. 2(c), exhibiting an extreme inhomogeneity, indicating a collapse stage.

It's obvious that the structure characteristics are very different between inverted pyramid and upright pyramid and three dimensional (3D) finite difference time domain (FDTD) analysis was carried out to gain insight into the light coupling in these two structures. The simulation dimensions of the inverted/upright pyramids (5 μm in width) were averaged from the values determined from the SEM images shown in Fig. 2(b). In the simulation, the electric field intensity ($|E|^2$) distribution of the electromagnetic (EM) wave is calculated using λ=631.57 nm, which is selected close to the peak irradiance of the solar spectra. The simulated results are shown in Fig. 3(a) and (b), respectively. It's evident that the majority energy of EM wave at 631.57 nm is limited inside of the inverted pyramids, which is much stronger than that in the upright pyramids. Light propagation paths in these two structures were also simulated by 3D ray tracing to interpret the FDTD simulation results [21–23]. The reflectance R of a given pyramidal surface can be expressed as the reflectances R_A, R_B...R_N of light rays reflected along a series of paths A, B...N, and the weightings f_A, f_B...f_N corresponding to each path depend on the surface geometry. These values define the probability that a ray will follow the relevant path. For upright pyramid, f_A~89% of normally incident rays undergo a double bounce (path A), and f_B~11% experience a triple bounce (path B) [23], as shown in Fig. 4(b). In case of inverted pyramid, see Fig. 4(a), f_A~59.26% follow a double bounce, but f_B~0.74% (path B) and f_C~40% (path C) suffer a triple bounce, this compares favourably to the 11% that suffer three bounces on upright pyramid [23]. Due to more incident rays experience a triple bounce on the front surface of inverted pyramid, so there is more chance for the reflected rays to re-enter the surface in inverted pyramid than in upright pyramid, therefore resulting in the energy of EM wave at 631.57 nm limited inside of the inverted pyramids is much stronger than that in the upright pyramids. The simulation findings reconfirm the superior photon harvesting ability of inverted pyramid.

Further reflectance spectra were recorded to compare light trapping properties of the samples, together with the simulations, see Fig. 5. The mean reflectivity of the raw p-Si (100) wafer is about 32% from 300 to 1000 nm and then decreases to about 12% when using upright pyramids. However, the average reflectivity decreased to 8% when the c-Si is Cu-etched in the solution for 10 min. As the etching time extends to 15 min, the reflectivity further decreased to as low as 5%. However, the reflectivity increased to 10% when further increases the etching time to 20 min since the inverted pyramid structures were overetched and became shallow. The reflectance spectrum's trend matches well with the samples' morphologies, and we can obtain different reflectance spectra by controlling the etching time. Importantly, the inverted pyramids show better AR ability than upright pyramids, consistent with the simulations. SiN_x is deposited to further reduce the reflectance of the solar cells. Fig. 5(b) shows the reflectance spectra with 80 nm SiN_x coating by 3D ray tracing simulations and experiments. Although there is a little deviation in the results between the simulations and experiments, they have similar trend and the simulation results can well explain the experimental results. The average reflectivity of sample B-15 is almost 1% lower than sample R at the wavelength range from 300 nm to 1000 nm, which also benefits from the inverted pyramid's triple bounce, according to the above interpretation, thus for the inverted pyramids structured samples, there is more destructive interference takes place at the SiN_x/Si interface, see Fig. 4, resulting in a relatively low reflectivity.

Moreover, the internal quantum efficiency (IQE) spectra, as shown in Fig. 5(b), show improved blue response of the inverted pyramids Si solar cell, suggesting that the inverted pyramids Si solar cells have enhanced light conversion properties [5]. In addition, the lifetime of the minority carriers for sample R is 4.49 μs, and it increased to 5.48 μs for sample B-15 (The samples used for the lifetime measurement are single side passivated by the SiN_x thin film). That is because these inverted pyramid structures are characterized with recessed and open deeps, making this texture very applicable for conformal SiN_x deposition, as shown in Fig. 5(c), thus resulting in sufficient surface passivation and reduced recombination losses. Fig. 5(d) exhibits the images of solar cells based on upright pyramids and inverted pyramids. It might be noted that the low carrier lifetime is due to the low quality of the raw Si wafer which were chosen by the producer at the factory where the experiments were carried out.

Table 1 compares the results for the three Cu-etched inverted pyramid Si solar cells to the otherwise-identical upright pyramid Si cells. The best performance was achieved on sample B-15, with the highest efficiency (E_{ff}) of 18.87% and the highest short-circuit current density (J_{sc}) of 37.47 mA/cm^2, compared to the upright pyramid Si cell E_{ff} of 18.40% and J_{sc} of 36.88 mA/cm^2, it indicates the advantages of superior light-trapping ability and structure characteristics for the inverted pyramid structure. It's worth mentioning that the contact resistance (R_s) of Si solar cells based on sample "Inverted Pyramids" exhibits lower than sample "Upright Pyramids". The contact formation between Ag electrode and Si takes place at the firing process. The glass frit in the Ag paste etches the SiN_x and removes a small part of the emitter region at a high temperature. Then the Ag in the dissolved glass frit recrystallizes in the etched emitter region during the cooling process [24]. As we know, R_s will be reduced by increasing the direct connection between Ag paste and the emitter region [24]. Fig. 6(a) and (b) show the SEM images of Ag electrode filling in the inverted pyramid structure. Due to the wide and open characteristic of inverted pyramid structure, an excellent filling of Ag electrode is formed even at the bottom, where there is almost no air void existed. A much clearer proof is exhibited in Fig. 6(c), the SEM image of Ag crystallites in the emitter region after immersing in nitric acid solution for 5 min. The Ag crystallites are distributed in the whole regions of the inverted pyramids, which indicates a good and compact connection with the emitter region.

4. Conclusion

In summary, an 18.87%-efficient inverted pyramid structured Si solar cell is achieved with V_{oc}, J_{sc} and FF of 637.7 mV, 37.47 mA/cm^2 and 78.84%, respectively, employing one-step Cu-assisted texturization technique. In comparison with a similar processed conventional upright pyramid Si cells, the Cu-etched inverted pyramid Si cells collect 0.59 mA/cm^2 more J_{sc} and 0.47% more E_{ff} on behalf of its superior light-trapping ability for absorbing more incident light and recessed structure characteristics for sufficient passivation and good ohm contact. Furthermore, as compared to the Ag-etched and Au-etched technique, the cost of the Cu-etched method is much lower. The results indicate that the inverted pyramid Si cells have enhanced light absorption and improved passivation and electrode contact. As such, our technique, compatible with current production line, is low-cost and simple, which may trigger a new era of solar cells based on inverted pyramid structured Si.

Acknowledgement

This work was supported by the Ministry of Science and Technology of China (Grant Nos. 2011CB302002 and 2009CB929404), the National Science Foundation of China (Grant Nos. 11174348, 51272280, 11274366, 61204067, and 61306011), the Chinese Academy of Sciences, and the Research Council of Norway in the framework of the IDEAS grant program administrated via the ENERGIX program, as well as OXYDERA equipment grant from the Centre for Materials Science and Nanotechnology at the University of Oslo.

References

[1] H.-C. Yuan, V.E. Yost, M.R. Page, P. Stradins, D.L. Meier, H.M. Branz, Efficient black silicon solar cell with a density-graded nanoporous surface: optical properties, performance limitations, and design rules, Appl. Phys. Lett. 95 (2009) 123501.
[2] Z. Huang, S. Zhong, X. Hua, X. Lin, X. Kong, N. Dai, W. Shen, An effective way to simultaneous realization of excellent optical and electrical performance in large-scale Si nano/microstructures: simultaneous realization of excellent optical and electrical performance, Prog. Photovolt. Res. Appl. 23 (2015) 964–972.
[3] K.Q. Peng, J.J. Hu, Y.J. Yan, Y. Wu, H. Fang, Y. Xu, S.T. Lee, J. Zhu, Fabrication of single-crystalline silicon nanowires by scratching a silicon surface with catalytic metal particles, Adv. Funct. Mater. 16 (2006) 387–394.
[4] Z. Huang, N. Geyer, P. Werner, J. de Boor, U. Gösele, Metal-assisted chemical etching of silicon: a review: in memory of Prof. Ulrich Gösele, Adv. Mater. 23 (2011) 285–308.
[5] F. Toor, H.M. Branz, M.R. Page, K.M. Jones, H.-C. Yuan, Multi-scale surface texture to improve blue response of nanoporous black silicon solar cells, Appl. Phys. Lett. 99 (2011) 103501.
[6] Y. Liu, T. Lai, H. Li, Y. Wang, Z. Mei, H. Liang, Z. Li, F. Zhang, W. Wang, A.Y. Kuznetsov, X. Du, Nanostructure formation and passivation of large-area black silicon for solar cell applications, Small 8 (2012) 1392–1397.
[7] H.M. Branz, V.E. Yost, S. Ward, K.M. Jones, B. To, P. Stradins, Nanostructured black silicon and the optical reflectance of graded-density surfaces, Appl. Phys. Lett. 94 (2009) 231121.
[8] J. Oh, H.-C. Yuan, H.M. Branz, An 18.2%-efficient black-silicon solar cell achieved through control of carrier recombination in nanostructures, Nat. Nanotechnol. 7 (2012) 743–748.
[9] Z.P. Huang, N. Geyer, L.F. Liu, M.Y. Li, P. Zhong, Metal-assisted electrochemical etching of silicon, Nanotechnology 21 (2010) 465301.
[10] H. Zheng, M. Han, P. Zheng, L. Zheng, H. Qin, L. Deng, Porous silicon templates prepared by Cu-assisted chemical etching, Mater. Lett. 118 (2014) 146–149.
[11] H. Morinaga, Mechanism of Metallic particle growth and metal-induced pitting on Si wafer surface in wet chemical processing, J. Electrochem. Soc. 141 (1994) 2834.
[12] J.-P. Lee, S. Choi, S. Park, Extremely superhydrophobic surfaces with micro- and nanostructures fabricated by copper catalytic etching, Langmuir 27 (2011) 809–814.
[13] N. Mitsugi, K. Nagai, Pit formation induced by copper contamination on silicon surface immersed in dilute hydrofluoric acid solution, J. Electrochem. Soc. 151 (2004) G302.
[14] K.Q. Peng, Y.J. Yan, S.P. Gao, J. Zhu, Dendrite-assisted growth of silicon nanowires in electroless metal deposition, Adv. Funct. Mater. 13 (2009) 127.
[15] Y.-T. Lu, A.R. Barron, Anti-reflection layers fabricated by a one-step copper-assisted chemical etching with inverted pyramidal structures intermediate between texturing and nanopore-type black silicon, J. Mater. Chem. A 2 (2014) 12043.
[16] F. Toor, J. Oh, H.M. Branz, Efficient nanostructured “black” silicon solar cell by copper-catalyzed metal-assisted etching, Prog. Photovolt. Res. Appl 23 (2014) 1375–1380.
[17] Y. Wang, L. Yang, Y. Liu, Z. Mei, W. Chen, J. Li, H. Liang, A. Kuznetsov, D. Xiaolong, Maskless inverted pyramid texturization of silicon, Sci. Rep. 5 (2015) 10843.
[18] L. Yang, Y. Liu, W. Chen, Y. Wang, H. Liang, Z. Mei, A. Kuznetsov, X. Du, Interface engineering of high efficiency organic-silicon heterojunction solar cells, ACS Appl. Mater. Interfaces 8 (2016) 26–30.
[19] E. Vazsonyi, K. De Clercq, R. Einhaus, E. Van Kerschaver, K. Said, J. Poortmans, J. Szlufcik, J. Nijs, Improved anisotropic etching process for industrial texturing of silicon solar cells, Sol. Energy Mater. Sol. Cells 57 (1999) 179–188.
[20] L. Yang, Y. Liu, Y. Wang, X. Li, W. Chen, Y. Hua, Q. Zhang, J. Fu, H. Liang, Z. Mei, X. Du, Optimization of silicon pyramidal emitter by self-selective Ag-assisted chemical etching, RSC Adv. 4 (2014) 24458.
[21] A.W. Smith, A. Rohatgi, Ray tracing analysis of the inverted pyramid texturing geometry for high efficiency silicon solar cells, Sol. Energy Mater. Sol. Cells 29 (1993) 37–49.
[22] S.C. Baker-Finch, K.R. McIntosh, One-dimensional photogeneration profiles in silicon solar cells with pyramidal texture, Prog. Photovolt. Res. Appl. 20 (2012) 51–61.
[23] S.C. Baker-Finch, K.R. McIntosh, Reflection of normally incident light from silicon solar cells with pyramidal texture, Prog. Photovolt. Res. Appl. 19 (2011) 406–416.
[24] H. Kim, S. Park, S.M. Kim, S. Kim, Y.D. Kim, S.J. Tark, D. Kim, Influence of surface texturing conditions on crystalline silicon solar cell performance, Curr. Appl. Phys. 13 (2013) S34–S40.